Effect of Humidity on Gas Sensing Performance of Carbon Nanotube Gas Sensors Operated at Room Temperature

Shooshtari, Mostafa; Salehi, Alireza; Vollebregt, Sten

DOI
10.1109/JSEN.2020.3038647

Publication date
2020

Document Version
Final published version

Published in
IEEE Sensors Journal

Effect of Humidity on Gas Sensing Performance of Carbon Nanotube Gas Sensors Operated at Room Temperature

Mostafa Shooshtari, Alireza Salehi, and Sten Vollebregt, *Senior Member, IEEE*

***Abstract*—Carbon nanotubes (CNTs) have shown promising results for gas sensing due to their high surface area. Since humidity has a great impact on the electrical conductivity of resistive CNT gas sensors, we have investigated the change of humidity on their sensing properties. In this study, we fabricated vertically aligned CNT-based gas sensors for the detection of volatile organic compounds. The morphologies and phase structures of the fabricated samples were characterized using scanning electron microscopy (SEM), X-ray diffraction (XRD) and Fourier-transform infrared spectroscopy (FT-IR), confirming the presence of CNT with some surface impurities. It was found that a relative humidity increase from 10% to 80% can reduce the electrical conductivity of the sensor by around 4%. On the other hand, for a humidity above 80% the conductivity increased slightly. The fabricated device has been used as a gas sensor for volatile organic compounds, and the cross-sensitivity to humidity was investigated. It was found that in the fabricated sensors, a change in humidity up to 80% results in a 40% decrease in the response for the studied organic compounds.**

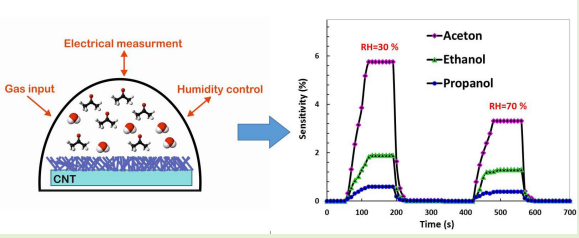

***Index Terms*—Carbon nanotubes, cross-sensitivity, gas sensors, humidity, volatile organic compounds.**

I. Introduction

HUMIDITY is one of the most important physical quantities which cannot be eliminated. Therefore, humidity sensors are the most widely used devices to measure the humidity for different applications. Humidity sensors are used in the industrial, environmental, and monitoring fields [1]–[4]. Corrosion caused by moisture is one of the most common causes of structural failure [5], so there is a great deal of research into the construction of high-efficiency humidity sensors. Humidity can affect all industrial equipment including measuring structures and disturb them [6]. Therefore, failure to control the amount of humidity can make the measurement system's responses unreliable. Gas sensors are one of the most important measurement systems in various industries. Various studies on different types of gas sensors have shown an unwanted effect of humidity on the responses to gases of interest [7]–[9].

Changes in the amount of humidity on different materials have different effects, depending on whether they are hydrophilic or hydrophobic materials [10]. The effect of humidity on hydrophilic materials can be macroscopic as well as microscopic while in the hydrophobic materials this effect is only visible microscopically [11]. These effects can cause changes in weight [12], capacitance [13], electrical resistance [14], thermal conductivity [15], crystal frequency [16], etc.

Carbon nanotubes (CNTs) are among the hydrophilic materials which are a kind of carbon allotrope [17]. CNTs, due to their electrical, mechanical, thermal, optical and sensing properties, are a good candidate for various sensors, including gas sensors, and are feasible to be integrated into electronic circuits [18]–[21]. The electrical properties of CNTs are sensitive to charge transfer and doping effects by interacting with molecules of sensible substances. The density of the charge carriers in the CNT can change when electron-withdrawing molecules or electron-donating molecules interact with the tubes. Furthermore, CNTs have a large surface area which can increase their sensitivity.

Manuscript received September 9, 2020; revised November 11, 2020; accepted November 12, 2020. Date of publication November 17, 2020; date of current version February 5, 2021. The associate editor coordinating the review of this article and approving it for publication was Prof. Minhee Yun. *(Corresponding author: Sten Vollebregt.)*

Mostafa Shooshtari and Alireza Salehi are with the Department of Electrical Engineering, K. N. Toosi University of Technology, Tehran 19697 64499, Iran (e-mail: m.shooshtari@tudelft.nl; salehi@kntu.ac.ir).

Sten Vollebregt is with the Laboratory of Electronic Components, Technology, and Materials, Delft University of Technology, 2628 CD Delft, The Netherlands (e-mail: S.Vollebregt@tudelft.nl).

Digital Object Identifier 10.1109/JSEN.2020.3038647

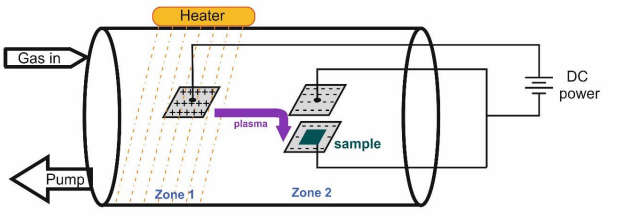

Fig. 1. The schematic diagram of PECVD setup for CNTs growth.

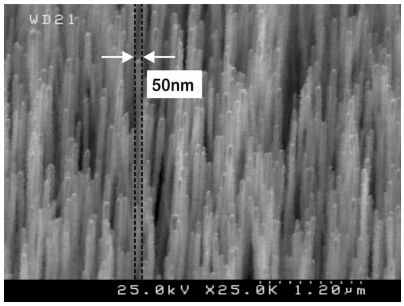

Fig. 2. SEM micrograph of CNTs grown on a 30 nm deposited nickel on a quartz substrate.

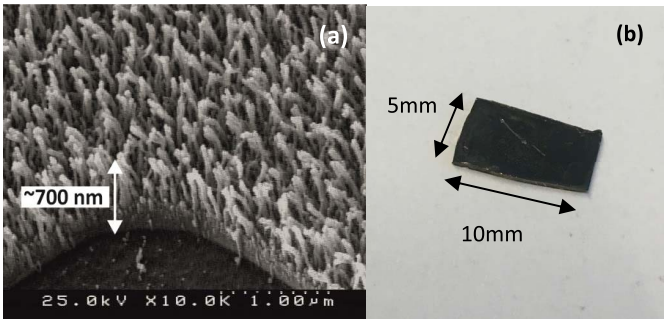

Fig. 3. (a) SEM micrograph of CNT sensor (Scale bar is 1 micron); (b) Example of a grown CNT sample.

In recent years, CNTs as humidity sensing layers have been investigated, and many researchers have reported the development of CNT-based sensors for humidity detection [22]. Generally, CNT humidity sensors are fabricated using bundles [23], hybrid polymer composites [24] or dispersed solutions [25] of single or multiwall carbon nanotubes. The performance of these sensors has been reported to be improved by the addition of suitable polymer or metal oxide nanoparticles [26].

However, limited work has been done on the effects of humidity on the gas sensing mechanism of CNTs [27], [28]. In this paper, vertically aligned MWCNTs have been synthesized on a quartz substrate via a simple, low-cost fabrication process. The effect of humidity on their electrical properties and Volatile Organic Compounds (VOCs) sensing has been investigated.

II. Experimental Methods

A. CNT Growth and Sensor Fabrication

Multi-walled carbon nanotubes (MWCNTs) were grown on a quartz substrate using plasma-enhanced chemical vapor deposition (PECVD) method. The method facilitated the growth of aligned MWCNTs by acquiring two temperature zones in the reaction chamber and applying a DC plasma between those two zones. The details of the method for growing MWCNTs are described in ref. [29]. As a catalyst, 10 to 30 nm of nickel thin film was deposited on a quartz substrate by the electron beam evaporation method. Vertical alignment was chosen for the CNTs to achieve the largest interaction surface. If CNTs were not vertically aligned, they would lean on each other and many of them would be isolated from the surface. Therefore, the volume-to-surface ratio decreases, and the diffusion of gas molecules becomes more difficult.

A schematic diagram of the PECVD reactor is shown in Fig. 1. As shown in the figure, the reactor chamber is separated into two different zones. Zone 1 was heated up to 600 °C and the temperature of zone 2 was set to 250 °C. The introduced acetylene reaction gas was dissociated by the heat and the plasma at the first zone (Z1) which then flows to the lower temperature zone (Z2) where the Ni coated substrates are placed. CNT growth takes place in zone 2 which is at a lower temperature, and which due to the electrode configuration led to the formation of a two-dimensional plasma. This two-dimensional plasma provides aligned CNTs. It should be noted that all reactions have been done at the absence of oxygen, thus, before starting the CNT growth process, the whole chamber must be pumped down to a low atmospheric pressure around 50 mTorr to evacuate atmospheric gasses.

A micrograph of the fabricated CNTs is shown in Fig.2. Regular formed CNTs of approx. 50 nm in diameter were obtained on the substrate. The aligned tubes result in a very high surface-to-volume ratio.

The sensors were fabricated by cutting out 10 mm wide, 5 mm long square samples. From scanning electron microscope images, the thickness of the samples is determined to be roughly 700 nm, as shown in Fig. 3(a). Copper wires were bonded as electrodes to the top of CNTs samples using silver paste. Fig. 3(b) shows the grown CNT sample before the wires were connected.

B. Measurements

Fourier-transform infrared spectroscopy (JASCO, model: 460 Plus) and X-ray diffraction (Inel, model: EQUINOX3000) were used to characterize the CNT samples.

All the humidity and gas experiments were carried out in a 1 liter chamber. To measure conductivity, a Keithley 238 source meter was used. A Pintek-900 LCR meter is used for testing the capacitance of the sensor. The relative humidity (RH) and temperatures inside the chamber were monitored. Relative humidity depends on temperature and the pressure of the system. In this study, because the subject is relative humidity, the temperature has been kept constant for a correct comparison. A Samwon commercial humidity meter was also used to measure the ambient humidity. The amount of humidity required for calibration was created by a commercial ultrasonic humidifier JR model JRG. A 1.6 MHz oscillator with 100 V output voltage was designed for the humidifier.

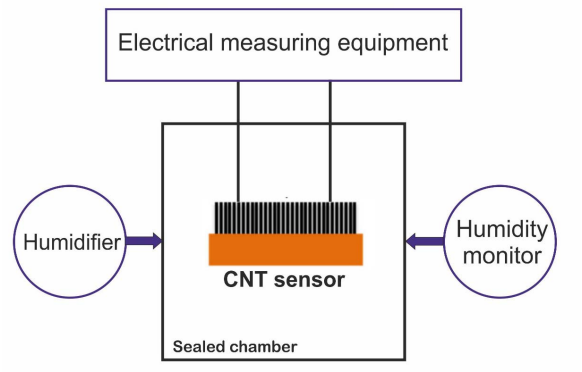

Fig. 4. Schematic diagram of the testing facility.

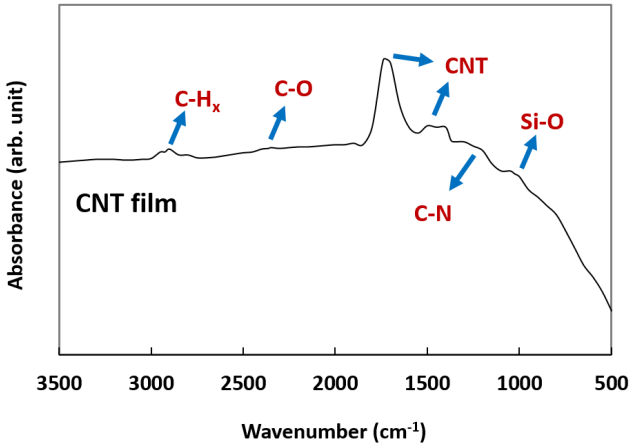

Fig. 5. FTIR spectra of the CNT samples produced by PECVD.

Silica gel was used to reduce the moisture content below ambient.

To characterize the performance of the fabricated aligned CNT used as a sensor, we measured the changes in its resistance and capacitance upon exposure to different gases and relative humidity's inside the chamber. Sensors response were obtained at the presence of VOCs vapors at different concentrations which were provided by evaporating an exact amount of liquid alcohol, which was measured by a micro sampler, into the chamber. As illustrated in Fig. 4, the fabricated sensor was placed inside the chamber and electronic measuring equipment was connected to the sensor outside of the chamber. Electrical measurements have been carried out with an accuracy of ±0.5%. Thus, a change in sensor resistance due to humidity is ruled out. All experiments are carried out at room temperature (24 °C ± 1 °C).

III. Results

A. Characterization

We applied Fourier-transform infrared (FTIR) spectroscopy and X-ray diffraction (XRD) to characterize the CNT samples. The results obtained by FTIR showed the formation of high purity product with the least amount of impurity. The FTIR spectroscopy also showed the presence of structures with graphite-like spectra, except that they are shifting towards lower wavenumbers [30]. Figure 5 shows a sequence of FTIR

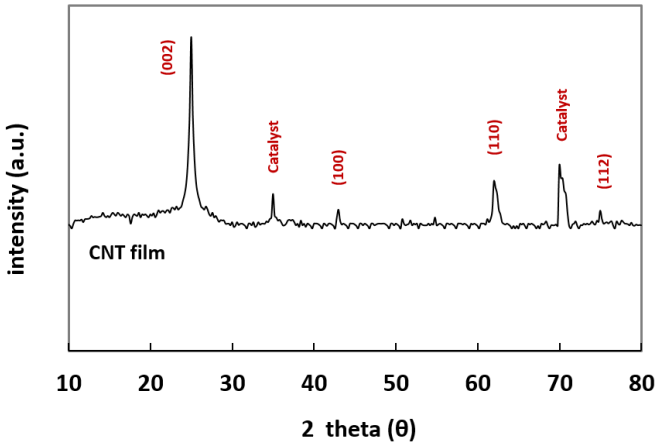

Fig. 6. X-ray diffraction pattern of aligned CNT film.

spectra for our CNT film for wavenumbers ranging between 500 cm^{-1} and 3500 cm^{-1}. As reported in [31], the peaks at 1736 cm^{-1} and 1445 cm^{-1} in the spectra are due to the stretching and bending vibration of the CNT. Peaks at 1736 cm^{-1} also show the highest absorption rate. Other absorption peaks are related to surface impurities resulting from the fabrication process. The spectra show dominant peaks at 2362, 1372, and 1250 cm^{-1}, which is corresponding to C–O, N–CH_3, CNT and C–N, respectively. The peaks at 2925 cm^{-1} and 2851 cm^{-1} are stretching vibrations of C-H_x. Furthermore, the peak observed at 1026 cm^{-1} is due to the vibration of the Si-O bond, which is related to the quartz (SiO_2) substrate.

The observed spectrum shows a small number of impurity bands with short intensity peak which indicates the high purity of the grown CNT. The observed spectrum corresponds to the graphs reported in the references [32], [33].

To analyze the phase response of CNT samples we use XRD. In our XRD equipment monochromatic optic Kα1 or Kα1/2 were used. The degree of X-ray radiation depends on the distances and location of atoms in the crystal lattice of the material [34]. We note that CNT do not have a crystalline lattice [35]. However, periodic structure results in the creation of diffraction peaks in the XRD diffraction. The XRD results measured at different angles confirmed the growth of CNT and its structural features [36]. The CNT X-ray pattern has many similarities to the graphite pattern because both are build-up from stacked graphene sheets [35].

The carbon atoms in the CNT, like other fullerenes, radiate rays in all directions. This variety of directions in different angles depends on the placement of the different graphite plates and the type of tube placement of the CNT. However, the peak intensity of CNT diffraction depends on the morphological direction of CNTs. When the X-ray strikes one of the walls of CNTs, it creates (002) peaks with some parallel reflections. In addition, as the X-rays pass through the gap between the walls or the tubes, it produces some hexagonal peak arrays [37].

Figure 6 shows the XRD pattern of the synthesized samples where the carbon peaks are well recognized [38]. As can be seen in the pattern, the peak (002) shows the existing carbon

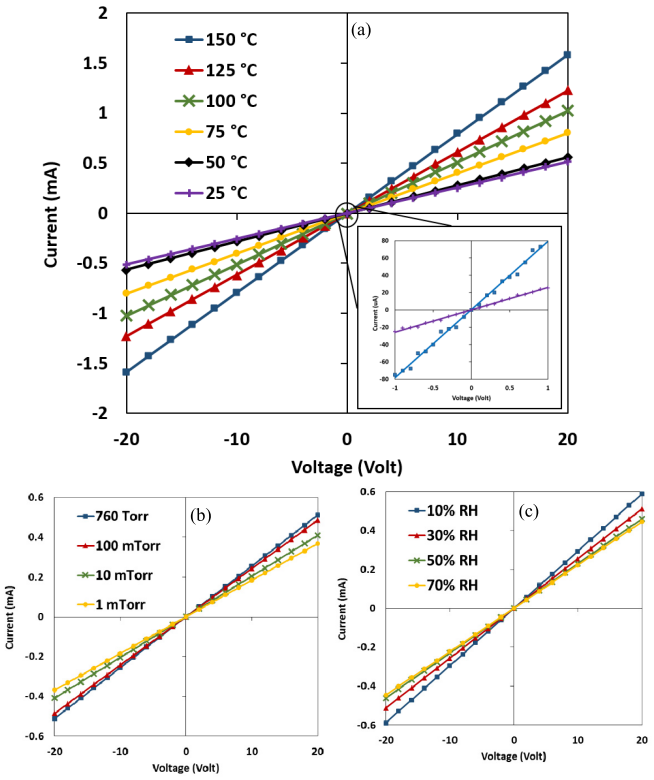

Fig. 7. I-V characteristic of aligned CNT at room condition with a change in a) temperature b) pressure c) relative humidity. The inset of a) shows the I-V characteristic for 25 °C and 150 °C from −1 V to +1 V), indicating good linearity and Ohmic contact. Unless otherwise specified the conditions are 25 °C, 760 Torr and 30% RH.

in the hexagonal atomic networks. This peak can also be the result of parallel stacking of carbon tube layers. It has been shown that peak (002) intensity decreases in aligned CNTs [39]. The distance between the carbon nanotube plates and the type of nanotube formation can affect the (002) peak [36]. Interestingly, the peak is also observed on the pattern of graphite plates [40]. The other peaks (100), (110) and (112) shown in the figure diffraction reflect the space between graphene plates and tubes. These distances also affect the magnitude and width of these peaks [36]. In addition to the known peaks in the X-ray diffraction of CNTs, several others are also observed. These peaks are due to the catalyst (nickel) used in the fabrication process which was observed in NiO form [41].

B. Conductivity Sensing Experiment

CNTs contain both electrons and holes but intrinsically typically behave as p-type semiconductors [42]. However, in some circumstances, they show metallic behaviors [43]. For instance, in aligned MWCNT, the CNT acts like metals because of their increased diameter which reduces the bandgap [44]. Also, their energy bands interactions will cause overlap of the conduction and valence bands. In other words, there is a high probability of having at least one metallic shell in MWCNT [45].

We now move on to the effect of peripheral factors on our samples. Figure 7 compares the current-voltage characteristic

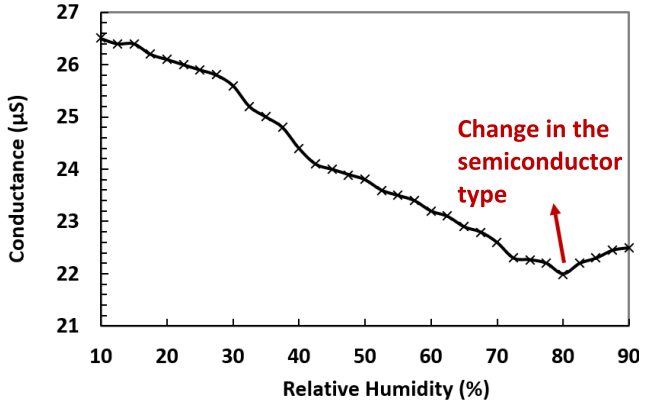

Fig. 8. The variation of the CNT sample conductance in terms of relative humidity at room temperature and atmospheric pressure.

of aligned CNTs for different ambient pressure, temperature, and humidity. As is shown, changing the humidity, pressure and temperature will not affect the CNT ohmic contacts with the silver electrodes. In all cases the devices behave Ohmic. The room conditions in this study assume 25 °C temperature, 760 Torr pressure and 30% relative humidity.

Since the CNTs are hydrophobic materials, their interaction with water molecules occurs at the microscopic level [17]. The presence of water molecules on the surface of the nanotubes can create surface groups such as –OH and –COOH. In MWCNTs, the bonds between the walls of the nanotube are sp^2 hybridization and there are π-bonds between the walls of the MWCNTs. Therefore, adsorption of water molecules occurs on the surface of the nanotube or between the walls and the electric charge transfer in this adsorption is a chemical process.

When CNTs inside the chamber are exposed to a certain amount of humidity, H_2O molecules are adsorbed on the surface of the nanotubes. The amount of this adsorption depends on the relative humidity. In the adsorption process, due to the difference in electric potential, electrons are transferred from the H_2O molecules to the CNT. As it is clear from Fig. 8, increasing the humidity reduces the electrical conductivity of the sensor and this reduction continues until a relative humidity of 80%. Electrons moving from the H_2O molecules to the CNT recombine with hole carriers of CNT. This recombination results in a decrease in the majority carriers of the CNT, which ends up to increasing the samples' resistance. Thus, H_2O molecules play the role of electron donor.

The upward trend after the 80% relative humidity can be due to two mechanisms: 1) A further increased electron impurity level results in more electron carriers than hole carriers. Therefore, at high humidity level, electrons become the majority carrier and CNT changes from a p-type semiconductor to an n-type semiconductor. Therefore, the increase in the number of electrons from adsorption leads to an increase in the electrical conductivity. Alternatively, 2) at high humidity a conductive electrolytic layer on the surface of the nanotube can form. Since this resistor is in parallel to the CNT resistor, the overall resistance is reduced.

The carrier transfer leads to a change in the Fermi level as well as an increase in the width of the depletion layer.

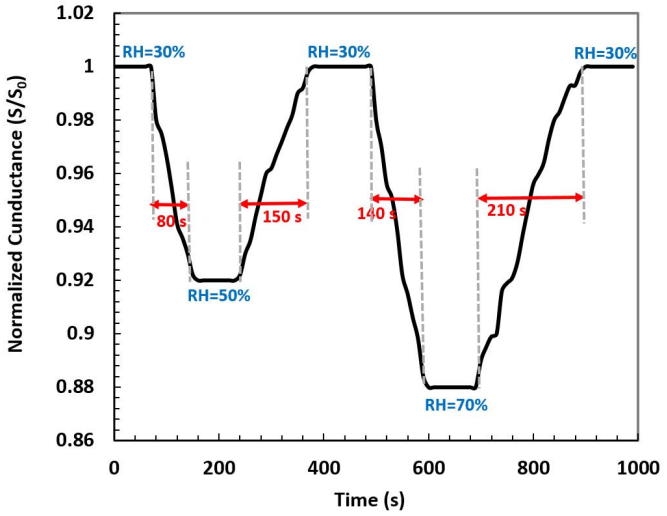

Fig. 9. Response and recovery curve of CNT sensor toward Relative Humidity (RH) with different levels at room temperature with 1.2 V DC bias.

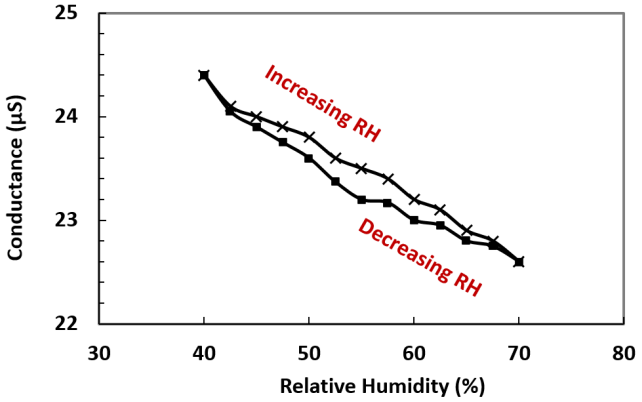

Fig. 10. Hysteresis loop of conductance increasing and decreasing for the Relative Humidity ranging from 40% to 70% at room temperature and atmospheric pressure.

Other than the carrier transfer, two other factors can affect the electrical conductivity: chemical reaction of hydrogen (-H^+ group) with the CNT surface oxygen (due to surface impurities) and a change in the intertube distance [46].

As is observed in Fig. 9, the CNT sensor is sensitive to changes in humidity. The figure also shows the response and the recovery time of the device toward relative humidity (RH) level from 30% to 50% and 70% at room temperature. Due to the adsorption of water molecules onto the CNT surface, the adsorption time occurs almost immediately at room condition. In contrast, the desorption time is longer. H_2O can adsorb on the surface and between the CNT walls.

In this study, we assumed that the response and recovery time criteria are 10% to 90%. The higher the humidity content, the adsorption on the surface of the nanotubes becomes more dominant and by cutting off the humidity, desorption of water molecules from the surface occurs faster. As it is clear from Fig. 9, the ratio of recovery time to response time from 70% to 30% compared to the same ratio from 50% to 30% is lower.

Within the adsorption and desorption process, there are several chemical mechanisms with different rates [47]. Since the change in conductivity depends on the rate of these mechanisms, the conductivity takes the form of a hysteresis curve. This phenomenon is depicted in Fig. 10, in which we have considered that the relative humidity varies from 40% to 70% and backwards.

C. Capacitance Sensing Experiment

The capillary condensation of water vapors is a common method for parameter evaluation for porous structural materials with a size of 2–100 nm [48]. The capillary condensation leads to the formation of water molecules between the walls of the nanotubes [49]. The trapped molecules do not just change the distance between the walls but modify the capacitance of the sample [50]. According to the equation $C = \varepsilon_0 \varepsilon_r \frac{A}{d}$, the measured capacitance of the sensor in our

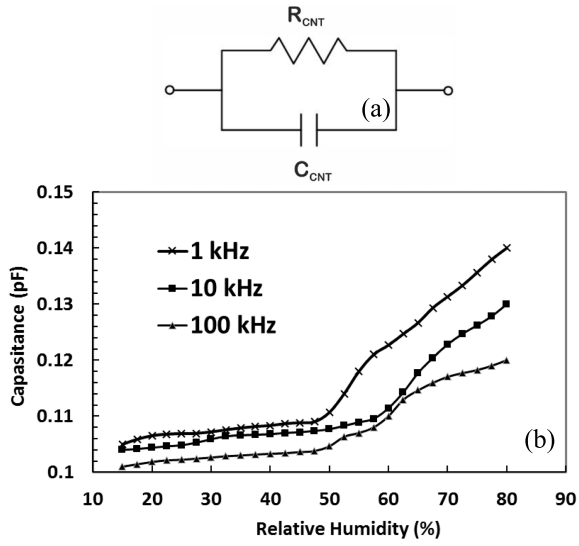

Fig. 11. a) Equivalent electrical circuit for CNT based humidity sensor. b) Variation of the CNT capacitance with relative humidity at different frequencies (1 kHz, 10 kHz and 100 kHz) at room temperature.

study is less than the capacitance of CNT humidity sensors previously reported in the literature [51]–[53], because the surface of the electrode is significantly smaller than the distance between electrodes. In CNT humidity sensors, a large area plate (A) is designed and the distance between the plated (d') is designed to be as small as possible but in our study, because both electrodes are placed on the CNT surface, the effective surface area (A) is very small.

The sensor was connected to an LCR meter. The LCR meter has a frequency range from 100 Hz to 100 kHz. Calibration was performed following the standard procedure of the LCR meter operation manual before starting the capacitance measurements. A bridge method technique was used in our LCR meter. A commercial capacitor sensor was used to eliminate the capacitive effects of other components. As a result, the equivalent circuit of the sensor can be modelled with a resistor R_{CNT} paralleled to a capacitor C_{CNT} as shown in Fig. 11(a). The measured values for R_{CNT} and C_{CNT} at room conditions are 39 kOhm and 0.1 pF, respectively.

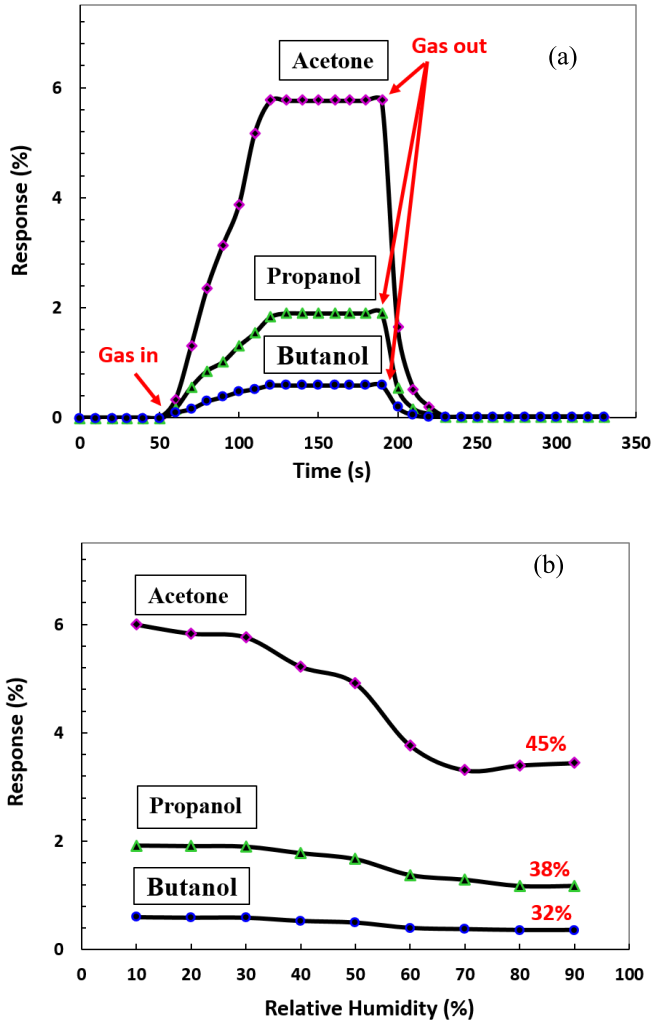

Fig. 12. a) response of CNT gas sensor at 50 ppm concentrations of butanol, propanol and acetone at room temperature and atmospheric pressure. b) The variation of the CNT sensor response in terms of relative humidity at the same conditions.

Figure 12(b) illustrates the variation of the capacitance as a function of relative humidity, for three different frequencies of 1 kHz, 10 kHz and 100 kHz. As the humidity increases the dielectric constant between the graphene plates changes when water moves between them. The relative permittivity from air to water increases and leads to larger capacitance. Additionally, and according to Fig. 11(b), it can be concluded from the figure that the rate of change in the capacitance is lower for higher frequencies. As the frequency increases, the response of the sensor decreases and the flat region shifts towards the higher humidity's. This is because the dielectric polarization of water vapor occurs properly at low frequencies [54].

D. Gas Sensing Experiment

The fabricated sensors are used for sensing different organic compounds such as vapor of Acetone, Butanol and Propanol. The following equation is used to calculate the response:

$$response(\%) = \frac{|R_{gas} - R_{air}|}{R_{air}} \times 100 \qquad (1)$$

TABLE I
HUMIDITY EFFECT ON GAS SENSING PARAMETERS AT ROOM TEMPERATURE

Gas	Concentration	Response @RH 30% [a]	Response @RH 70%	Response and recovery time @RH 30%	Response and recovery time @RH 70%
Acetone	50 ppm	5.764	3.310	~ 50 s	~ 30 s
Propanol	50 ppm	1.899	1.293	~ 65 s	~ 30 s
Butanol	50 ppm	0.589	0.376	~ 65 s	~ 40 s
Acetone	200 ppm	8.011	4.600	~ 200 s	~ 110 s
Propanol	200 ppm	2.601	1.773	~ 250 s	~ 125 s
Butanol	200 ppm	0.801	0.512	~ 260 s	~ 150 s

[a]Gas Response to 30% humidity

In which R_{air} is the resistance of two ends of the terminals before gas exposure in stable mode and R_{gas} is the exact resistance after gas exposure.

Figure 12(a) shows the response of the fabricated sensor at room condition with a relative humidity of approximately 30%, for 50 ppm of different gases. Gas sensing is also considered for relative humidity ranging from about 10% to 90%. As indicated in Fig. 12(b) the response of the sensor to the studied gases decreases as the humidity increases. The decrease in the response is slow for a relative humidity below 50%, while after that variations continue with a steeper slope.

Since the reduction in gas sensing of CNT occurs because of the adsorption of surface oxygen, presence of water vapor molecules on the surface of the nanotubes reduces the surface to volume area of the gas sensor and causes less oxygen to be targeted when exposed to gaseous molecules. We also note that it is less likely for these molecules to pass through the walls due to the water filling between the walls. The greater effect of acetone than other vapors can be due to a large affinity for water adsorption of acetone [55].

Although the change of semiconductor type of the CNTs occurs at the relative humidity above 80% as shown in Fig. 8, since the volume of water vapor molecules on the surface of the nanotubes is remarkably large, the postulated type changing does not have a significant effect on gas sensing.

In the operating frequency range of gas sensors (usually DC to a maximum of 100 kHz) the effect of reactance resistance is negligible (the imaginary part of the impedance is negligible). In this study, the impedance phase varies from 0 to 1.5 degree, which is practically trivial.

Table I shows the results of the humidity effect on gas sensing parameters in the fabricated CNT sensors. As shown, 40% increase in humidity results in about 60% decrease in response for all studied gases. This increase in humidity has no adverse effect on response time and recovery time of sensors.

Based on the information obtained in this study, the use of a CNT gas sensor should be done considering the effect of humidity. Humidity changes in the environment make the sensory response of CNT gas sensor unreliable. Use of other CNT structures or hybrid structures with materials that can reduce the effect of humidity can be a solution to this limitation. An array of CNT sensors that can detect the effects of humidity by processing and patterning their results is another solution.

IV. Conclusion

Changes in ambient relative humidity can affect the electrical conductivity, capacitance and sensing mechanism of CNT sensors. In this study, aligned CNT which function as sensing layer with a large surface-to-volume ratio were grown on quartz substrate by using PECVD. FTIR and XRD characterization techniques and SEM images were used to characterize the samples and CNT growth was confirmed. The fabricated aligned CNT sample was investigated as a resistive and capacitive humidity sensor and its equivalent circuit model was presented. The effect of humidity on different concentrations of propanol, butanol and acetone volatile organic compounds were tested. It has been determined that changes in humidity can alter the CNT sensor sensing response to the mentioned gases and the effect of humidity cannot be ignored.

References

[1] D. Lo Presti, C. Massaroni, and E. Schena, "Optical fiber gratings for humidity measurements: A review," *IEEE Sensors J.*, vol. 18, no. 22, pp. 9065–9074, Nov. 2018.

[2] L. S. M. Alwis, H. Bustamante, B. Roth, K. Bremer, T. Sun, and K. T. V. Grattan, "Evaluation of the durability and performance of FBG-based sensors for monitoring moisture in an aggressive gaseous waste sewer environment," *J. Lightw. Technol.*, vol. 35, no. 16, pp. 3380–3386, Aug. 15, 2017.

[3] F. Ricciardella, S. Vollebregt, T. Polichetti, P. M. Sarro, and G. S. Duesberg, "Low-humidity sensing properties of multi-layered graphene grown by chemical vapor deposition," *Sensors*, vol. 20, no. 11, p. 3174, Jun. 2020.

[4] A. Salehi, A. Nikfarjam, and D. J. Kalantari, "Highly sensitive humidity sensor using Pd/Porous GaAs Schottky contact," *IEEE Sensors J.*, vol. 6, no. 6, pp. 1415–1421, Dec. 2006.

[5] R. Zhang, J. Zhang, R. Schmidt, J. Gilbert, and B. Guo, "Effects of moisture content, temperature and pollutant mixture on atmospheric corrosion of copper and silver and implications for the environmental design of data centers (RP-1755)," *Sci. Technol. Built Environ.*, vol. 26, no. 4, pp. 567–586, Apr. 2020.

[6] A. Staerz, C. Berthold, T. Russ, S. Wicker, U. Weimar, and N. Barsan, "The oxidizing effect of humidity on WO3 based sensors," *Sens. Actuators B, Chem.*, vol. 237, pp. 54–58, Dec. 2016.

[7] H.-Y. Li, C.-S. Lee, D. H. Kim, and J.-H. Lee, "Flexible room-temperature NH3 sensor for ultrasensitive, selective, and humidity-independent gas detection," *ACS Appl. Mater. Interfaces*, vol. 10, no. 33, pp. 27858–27867, Aug. 2018.

[8] A. Nasriddinov *et al.*, "Effect of humidity on light-activated no and NO_2 gas sensing by hybrid materials," *Nanomaterials*, vol. 10, no. 5, p. 915, 2020.

[9] M. Eslamian, E. Nadimi, and A. Salehi, "Effect of humidity on gas sensing properties of tin dioxide toward carbon monoxide: A first principle study," in *Proc. Iranian Conf. Electr. Eng. (ICEE)*, May 2017, pp. 276–278.

[10] K. Fukuda, S. L. Sheng, and Z. A. Subhi, "Tribological behavior of hydrophilic and hydrophobic surfaces in atmosphere with different relative humidity," *Tribol. Online*, vol. 14, no. 5, pp. 353–358, 2019.

[11] J. Škvarla, "Hydrophobic interaction between macroscopic and microscopic surfaces. Unification using surface thermodynamics," *Adv. Colloid Interface Sci.*, vol. 91, no. 3, pp. 335–390, Jul. 2001.

[12] R. Cardoso, G. Sarapajevaite, O. Korsun, S. Cardoso, and L. Ilharco, "Sol-gel relative humidity sensors: Impact of electrode geometry on performance in soil suction measurements," *J. Sensor Technol.*, vol. 07, no. 01, pp. 1–23, 2017.

[13] T. A. Blank, L. P. Eksperiandova, and K. N. Belikov, "Recent trends of ceramic humidity sensors development: A review," *Sens. Actuators B, Chem.*, vol. 228, pp. 416–442, Jun. 2016.

[14] I. Rahim *et al.*, "Capacitive and resistive response of humidity sensors based on graphene decorated by PMMA and silver nanoparticles," *Sens. Actuators B, Chem.*, vol. 267, pp. 42–50, Aug. 2018.

[15] C. Dubey and B. Kumar, "Organic humidity sensors with different materials and its application in environment monitoring," in *Proc. 5th IEEE Uttar Pradesh Sect. Int. Conf. Electr., Electron. Comput. Eng. (UPCON)*, Nov. 2018, pp. 1–6.

[16] H. Jin *et al.*, "A humidity sensor based on quartz crystal microbalance using graphene oxide as a sensitive layer," *Vacuum*, vol. 140, pp. 101–105, Jun. 2017.

[17] Z. Zhou *et al.*, "Parahydrophobicity and stick-slip wetting dynamics of vertically aligned carbon nanotube forests," *Carbon*, vol. 152, pp. 474–481, Nov. 2019.

[18] M. M. Rana, D. S. Ibrahim, M. R. Mohd Asyraf, S. Jarin, and A. Tomal, "A review on recent advances of CNTs as gas sensors," *Sensor Rev.*, vol. 37, no. 2, pp. 127–136, Mar. 2017.

[19] S. Vollebregt, F. Tichelaar, H. Schellevis, C. Beenakker, and R. Ishihara, "Carbon nanotube vertical interconnects fabricated at temperatures as low as 350 °C," *Carbon*, vol. 71, pp. 249–256, May 2014.

[20] R. Arsat, X. He, P. Spizzirri, M. Shafiei, M. Arsat, and W. Wlodarski, "Hydrogen gas sensor based on highly ordered polyaniline/multiwall carbon nanotubes composite," *Sensor Lett.*, vol. 9, no. 2, pp. 940–943, Apr. 2011.

[21] C. Piloto *et al.*, "Room temperature gas sensing properties of ultrathin carbon nanotube films by surfactant-free dip coating," *Sens. Actuators B, Chem.*, vol. 227, pp. 128–134, May 2016.

[22] X. Zhang *et al.*, "Novel printed carbon nanotubes based resistive humidity sensors," in *Proc. IEEE Int. Conf. Flexible Printable Sensors Syst. (FLEPS)*, Jul. 2019, pp. 1–3.

[23] V. Turkani, D. Maddipatla, B. Narakathu, B. Bazuin, and M. Atashbar, "A fully printed CNT based humidity sensor on flexible PET substrate," in *Proc. 17th Int. Meeting Chem. Sens. (IMCS)*, 2018, pp. 519–552.

[24] B. Cai *et al.*, "Semiconducting single-walled carbon nanotube/graphene van der Waals junctions for highly sensitive all-carbon hybrid humidity sensors," *J. Mater. Chem. C*, vol. 8, no. 10, pp. 3386–3394, 2020.

[25] X. Li, X. Chen, X. Chen, X. Ding, and X. Zhao, "High-sensitive humidity sensor based on graphene oxide with evenly dispersed multi-walled carbon nanotubes," *Mater. Chem. Phys.*, vol. 207, pp. 135–140, Mar. 2018.

[26] K. N. Chappanda, O. Shekhah, O. Yassine, S. P. Patole, M. Eddaoudi, and K. N. Salama, "The quest for highly sensitive QCM humidity sensors: The coating of CNT/MOF composite sensing films as case study," *Sens. Actuators B, Chem.*, vol. 257, pp. 609–619, Mar. 2018.

[27] C. Struzzi *et al.*, "Exploiting sensor geometry for enhanced gas sensing properties of fluorinated carbon nanotubes under humid environment," *Sens. Actuators B, Chem.*, vol. 281, pp. 945–952, Feb. 2019.

[28] C. Cantalini, L. Valentini, I. Armentano, L. Lozzi, J. Kenny, and S. Santucci, "Sensitivity to NO_2 and cross-sensitivity analysis to NH_3, ethanol and humidity of carbon nanotubes thin film prepared by PECVD," *Sens. Actuators B, Chem.*, vol. 95, pp. 195–202, Oct. 2003.

[29] M. K. Tabatabaei, H. Ghafouri Fard, J. Koohsorkhi, S. Khatami, and S. Mohajerzadeh, "Remote and direct plasma regions for low-temperature growth of carbon nanotubes on glass substrates for display applications," *J. Phys. D, Appl. Phys.*, vol. 44, no. 11, Mar. 2011, Art. no. 115401.

[30] S. M. Jain, F. Cesano, D. Scarano, and T. Edvinsson, "Resonance Raman and IR spectroscopy of aligned carbon nanotube arrays with extremely narrow diameters prepared with molecular catalysts on steel substrates," *Phys. Chem. Chem. Phys.*, vol. 19, no. 45, pp. 30667–30674, 2017.

[31] V. Ţucureanu, A. Matei, and A. M. Avram, "FTIR spectroscopy for carbon family study," *Crit. Rev. Anal. Chem.*, vol. 46, no. 6, pp. 502–520, Nov. 2016.

[32] L. Carson *et al.*, "Synthesis and characterization of chitosan–carbon nanotube composites," *Mater. Lett.*, vol. 63, pp. 617–620, Mar. 2009.

[33] A. Misra, P. K. Tyagi, M. K. Singh, and D. S. Misra, "FTIR studies of nitrogen doped carbon nanotubes," *Diamond Rel. Mater.*, vol. 15, nos. 2–3, pp. 385–388, Feb. 2006.

[34] B. E. Carlsten, "Tutorial on X-ray free-electron lasers," *IEEE Trans. Plasma Sci.*, vol. 46, no. 6, pp. 1900–1912, Jun. 2018.

[35] T. Belin and F. Epron, "Characterization methods of carbon nanotubes: A review," *Mater. Sci. Eng., B*, vol. 119, no. 2, pp. 105–118, 2005.

[36] R. Das, S. Bee Abd Hamid, M. Eaqub Ali, S. Ramakrishna, and W. Yongzhi, "Carbon nanotubes characterization by X-ray powder diffraction—A review," *Current Nanosci.*, vol. 11, no. 1, pp. 23–35, 2015.

[37] Z. Q. Li, C. J. Lu, Z. P. Xia, Y. Zhou, and Z. Luo, "X-ray diffraction patterns of graphite and turbostratic carbon," *Carbon*, vol. 45, no. 8, pp. 1686–1695, Jul. 2007.

[38] H. Soleimani *et al.*, "Impact of carbon nanotubes based nanofluid on oil recovery efficiency using core flooding," *Results Phys.*, vol. 9, pp. 39–48, Jun. 2018.
[39] Q. Jiang, Q. Zhang, X. Wu, L. Wu, and J.-H. Lin, "Exploring the interfacial phase and $\pi--\pi$ stacking in aligned carbon nanotube/polyimide nanocomposites," *Nanomaterials*, vol. 10, no. 6, p. 1158, 2020.
[40] R. Siburian, H. Sihotang, S. Lumban Raja, M. Supeno, and C. Simanjuntak, "New route to synthesize of graphene nano sheets," *Oriental J. Chem.*, vol. 34, no. 1, pp. 182–187, Feb. 2018.
[41] W. H. Tan, S. L. Lee, and C. T. Chong, "TEM and XRD analysis of carbon nanotubes synthesised from flame," in *Key Engineering Materials*. 2017, pp. 470–475.
[42] J. L. Blackburn, A. J. Ferguson, C. Cho, and J. C. Grunlan, "Carbon-nanotube-based thermoelectric materials and devices," *Adv. Mater.*, vol. 30, no. 11, 2018, Art. no. 1704386.
[43] I. Stavarache *et al.*, "Electrical behavior of multi-walled carbon nanotube network embedded in amorphous silicon nitride," *Nanoscale Res. Lett.*, vol. 6, no. 1, pp. 1–6, 2011.
[44] W. B. Choi *et al.*, "Aligned carbon nanotubes for nanoelectronics," *Nanotechnology*, vol. 15, no. 10, p. S512, 2004.
[45] S. Vollebregt and R. Ishihara, "Carbon nanotubes as vertical interconnects for 3D integrated circuits," in *Carbon Nanotubes for Interconnects*. Cham, Switzerland: Springer, 2017, pp. 195–213.
[46] K.-P. Yoo, L.-T. Lim, N.-K. Min, M. J. Lee, C. J. Lee, and C.-W. Park, "Novel resistive-type humidity sensor based on multiwall carbon nanotube/polyimide composite films," *Sens. Actuators B, Chem.*, vol. 145, no. 1, pp. 120–125, Mar. 2010.
[47] D. Jung, M. Han, and G. S. Lee, "Humidity-sensing characteristics of multi-walled carbon nanotube sheet," *Mater. Lett.*, vol. 122, pp. 281–284, May 2014.
[48] A. V. Neimark and P. I. Ravikovitch, "Capillary condensation in MMS and pore structure characterization," *Microporous Mesoporous Mater.*, vols. 44–45, pp. 697–707, Apr. 2001.
[49] Z. Zhao, J. Zhang, J. Zhang, C. Li, Y. Li, and X. Wang, "Capacitance-type MWCNTs/SiO2 humidity sensor based on capillary condensation and percolation theory," *Sens. Actuators A, Phys.*, vol. 263, pp. 648–653, Aug. 2017.
[50] W.-P. Chen, Z.-G. Zhao, X.-W. Liu, Z.-X. Zhang, and C.-G. Suo, "A capacitive humidity sensor based on multi-wall carbon nanotubes (MWCNTs)," *Sensors*, vol. 9, no. 9, pp. 7431–7444, Sep. 2009.
[51] S. K. Reddy, I. Gendelis, and A. Ya'akobovitz, "Vertically aligned carbon nanotubes capacitive sensors," *IEEE Sensors J.*, vol. 19, no. 12, pp. 4375–4380, Jun. 2019.
[52] H. Kim *et al.*, "Multifunctional SENSING using 3D printed CNTs/BaTiO3/PVDF nanocomposites," *J. Composite Mater.*, vol. 53, no. 10, pp. 1319–1328, May 2019.
[53] X. Yang, Y. Wang, and X. Qing, "A flexible capacitive sensor based on the electrospun PVDF nanofiber membrane with carbon nanotubes," *Sens. Actuators A, Phys.*, vol. 299, Nov. 2019, Art. no. 111579.
[54] D. Zhang, H. Chang, P. Li, R. Liu, and Q. Xue, "Fabrication and characterization of an ultrasensitive humidity sensor based on metal oxide/graphene hybrid nanocomposite," *Sens. Actuators B, Chem.*, vol. 225, pp. 233–240, Mar. 2016.
[55] F. U. Nigiz and N. D. Hilmioglu, "Removal of acetone from wastewater by POSS loaded PDMS membrane," *Periodica Polytechnica Chem. Eng.*, vol. 61, no. 13, pp. 163–170, 2017.

Mostafa Shooshtari is currently pursuing the Ph.D. degree in electrical engineering with the K. N. Toosi University of Technology, Tehran, Iran. He is also a Guest Researcher with the EKL Laboratory, Delft University of Technology, Delft, The Netherlands. His research interests include nanostructured gas sensors and semiconductor devices.

Alireza Salehi is a Full Professor with the K. N. Toosi University of Technology. He manages the Semi-Conductor Laboratory in which different research projects have been done. His research interests include biosensors and gas sensors based on nanostructures and solar cells.

Sten Vollebregt (Senior Member, IEEE) received the M.Sc. *(cum laude)* degree and the Ph.D. degree in electrical engineering from the Delft University of Technology, in 2009 and 2014, respectively. Since October 2017, he has been an Assistant Professor with the Laboratory of Electronic Components, Technology and Materials, Delft University of Technology, where his research focuses on the integration of emerging electronic materials into semiconductor technology for sensing applications. His research interests include (carbon-based) nanomaterials, 3D monolithic integration, wide-bandgap semiconductors, and (harsh) environmental sensors.